Concentric-Ring and Sector-Vortex Phased-Array Applicators for Ultrasound Hyperthermia

CHARLES A. CAIN, SENIOR MEMBER, IEEE, AND SHIN-ICHIRO UMEMURA

Abstract—Concentric-ring phased arrays subdivided into sectors (radial slices) can, with appropriate phasing, produce power absorption patterns useful for hyperthermia cancer therapy. The ability of a concentric-ring array to move a focal region along the central axis of the transducer is well known. Less well known is the ability of such an array to produce variable diameter annular (or ring) focal regions. Such focal rings can be effective in heating some tumors if directed around the tumor periphery. These focal rings have been produced in the past by fixed annular focus lenses, or effectively by mechanical scanning of "point" focus ultrasonic transducers. Production of these focal rings by a concentric-ring phased array has the advantage of allowing the focal ring diameter and focal length to be easily changed and scanned by phasing providing much greater heating flexibility. However, under some conditions such arrays produce very large secondary focus effects along the central axis of the array. Concentric-ring arrays can also provide only patterns of circular symmetry. These problems can be partially solved by dividing the disk of the array into sectors. By appropriate phasing of the sectors, the intensity along the central axis can be greatly reduced. Moreover, appropriate phasing of the rings and sectors can produce patterns that are circularly asymmetric. By controlling these asymmetries, nonspherical tumors can be heated more optimally. Power absorption patterns in lossy media for this class of applicators are analyzed numerically allowing a quantitative evaluation of both advantages and limitations of this approach. A thermal model based on the bioheat equation is also used to predict temperature distributions in volumes where important thermal parameters, particularly blood flow, are varied.

I. INTRODUCTION

THE PRIMARY task of any hyperthermia applicator should be to raise the temperature throughout a tumor volume above some minimum therapeutic temperature. This should be accomplished while maintaining the maximum temperatures in normal tissue and in the tumor below acceptable values usually determined by thresholds for normal tissue damage and pain, respectively. For a given set of anatomical and physiological parameters, there may be a range of power deposition patterns that will result in appropriate temperature distributions within the treatment volume. The range of the set of acceptable power deposition patterns may change significantly during treatment, particularly due to changes in blood flow. The ability to adapt quickly to such changes is a major advantage of the use of phased arrays in hyperthermia applicator design.

Manuscript received September 18, 1985; revised December 13, 1985.

C. A. Cain is with the Department of Electrical and Computer Engineering, Bioacoustics Research Laboratory, University of Illinois, Urbana, IL 61801.

S.-I. Umemura is with Hitachi Central Research Laboratory, Ltd., Kokubunji, Tokyo 185, Japan.

IEEE Log Number 8607843.

Phased array applicators based on ultrasonic [1]–[3] and electromagnetic [4]–[6] heating have been studied. In this paper, a new class of ultrasonic phased-array applicators is investigated.

It has been well established on theoretical, as well as experimental grounds, that energy deposition around the periphery of moderately perfused tumors results in more uniform tumor temperature distributions than that produced by uniform power deposition within the tumor volume [7]–[9]. This mode of heating could be achieved by one of several techniques, such as aiming several focused transducers at points around the periphery [10], scanning a spot focus around the periphery by mechanical [7] or electrical [1]–[4] means, or using a specially designed lens with an annular or ring-shaped focus [9], [11].

The major disadvantage of fixed-lens annular-focus transducers is the inflexibility of such systems resulting from the fixed diameter and focal length of the heating annulus. Mechanical scanning of fixed, single-focus applicators offers greater flexibility, however, such systems are cumbersome and not fast enough to prevent significant temporal variations in temperature (thermal ripple). Electrical scanning of a spot focus using two-dimensional phased arrays, stacked linear-phased arrays [1], [2], or tapered linear-phased arrays [3], has the advantage of speed and flexibility but suffers from the need for many elements to prevent significant grating lobe formation resulting from the large scan angles required in such systems [1].

The phased-array applicator system proposed herein synthesizes an annular focal region directly without the added complexity of first synthesizing a spot and then scanning it in a circular path to obtain the desired heating pattern. The applicator is similar to axial focus concentric-ring transducers used for dynamic focusing in diagnostic imaging systems [12] or therapeutic hyperthermia [13], [14]. However, the phasing of the rings can be adjusted to synthesize variable diameter focal annuli at a depth that also can be scanned electrically. Thus, heating rings that can be rapidly scanned in diameter and focal length are obtained using far fewer elements and associated driving hardware.

There are, however, several disadvantages of the concentric-ring applicator system for hyperthermia. Only focal

0018-9480/86/0500-0542$01.00 ©1986 IEEE

regions of circular symmetry can be synthesized. Moreover, the applicator generates the strong secondary focus along the central axis first described by Beard *et al.* [9]. This problem becomes particularly severe when small annuli at depth are required. A partial solution to this problem can be obtained by dividing the concentric-ring applicator into sectors (pie slices) and by appropriate phasing of the sectors. If the sectors are driven by a "wave" of the form $e^{j[\omega t+\phi(\theta)]}$, then it will be shown that an annular focus of small radius is produced when $\phi(\theta)=m\theta$ where m is an integer and θ is the angular position around the circular array. Moreover, because of symmetry considerations, the intensity along the central axis is theoretically zero. By certain other choices for $\phi(\theta)$, one can obtain a form of spatial frequency modulation around the array which, as will be demonstrated, produces circularly asymmetric "enlongated ring" focal regions. Because this form of phasing produces the equivalent of a rotating excitation wave on the face of the transducer with the resultant cyclone-shaped focal region, it is referred to henceforth as a "sector-vortex" applicator. Both the concentric-ring and sector-vortex applicators are analyzed in what follows.

II. Array Descriptions

A. Concentric-Ring Array

A concentric-ring array is illustrated in Fig. 1. The array consists of N rings each of width d. The distance from the center of each ring to the array center is given by r_k, $k=1,2,\cdots,N$. Each ring is driven by a continuous sinusoidal signal with phase ϕ_k with respect to the source or reference oscillator. Fig. 1(a) shows one possible configuration where a separate power amplifier drives each ring with a signal, which has been appropriately phase-shifted. In this paper, the amplifier gains A_k are all assumed to be equal. The phase shifts ϕ_k could be generated digitally using n-bit programmable counters assuming that the input driving frequency is $n\omega_o$ where ω_o is the desired output frequency [15].

To generate an annular focal region, it is necessary to achieve a proper phase distribution ϕ_k over the set of array rings. If the desired heating annulus has a focal length F and a radius R from the center of the focal plane (see Fig. 1(b)), and if contributions from only the proximal half of the array are considered, then simple geometric arguments give the required phase distribution ϕ_k as

$$\phi_k = -\frac{\omega_o\sqrt{F^2+(R-kd)^2}}{c} \tag{1}$$

where ω_o is the frequency of the source oscillator and c is the speed of sound in the medium to be heated. If d is made arbitrarily small and the diameter of the array remains fixed, then the criterion given by (1) results in production of the same annular focal regions produced by fixed lens systems. The assumption of arbitrarily small ring width is made in the work which follows.

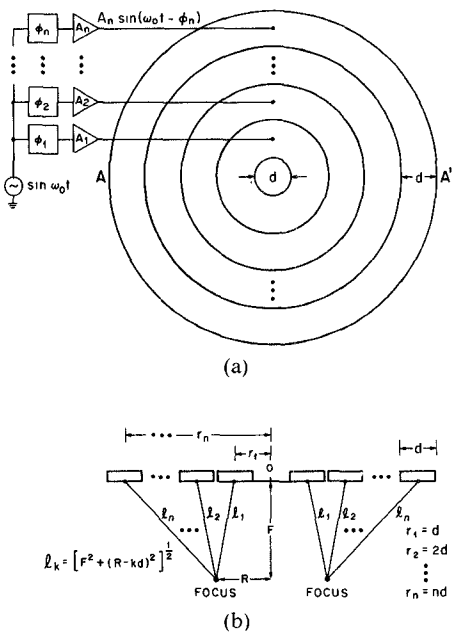

Fig. 1. Schematic of concentric-ring array. (a) Top view. (b) Cross section through AA'.

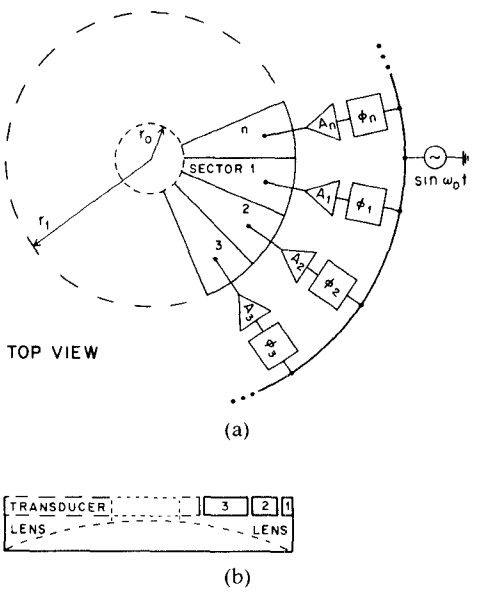

Fig. 2. Schematic of sector-vortex array. (a) Top view. (b) Edge view.

B. Sector-Vortex Array

The sector-vortex array consists of a transducer disk of radius r_1 divided into N sectors of equal size as illustrated in Fig. 2(a). Unless otherwise specified, it is assumed herein that the segmented disk is associated with a concave-converging acoustic lens of radius r_1, and focal length Z_f (Fig. 2(b)). In some applications, it is desirable to remove the array center to a radius r_o creating a doughnut-shaped applicator with geometric focusing.

A cylindrical coordinate system (r,θ) on the applicator and (R,ψ) in the focal plane, is assumed. The phase distribution ϕ_t over the N sectors is given by

$$\phi_t = m[\theta_t+\beta(\theta_t)] \tag{2}$$

for $i=1,2,\cdots,N$ where m is the vortex mode number, $\theta_t = i2\pi/N$, and $\beta(\theta)$ is a phase modulation function, the significance of which will become apparent. From symmetry considerations, it is seen that a transducer so phased will always produce zero intensity along the central axis, a useful consideration for some hyperthermia applications.

The complex amplitude of the driving signal for the i-th element can be written as

$$A(\theta_t) = A_o \exp j\{m[\theta_t + \beta(\theta_t)] - \omega_o t\} \tag{3}$$

where A_o is a constant. The phase distribution over the N sectors is such that an excitation field rotates around the disk at a phase velocity ω_p where

$$\omega_p = \frac{\omega_o}{m}\left[1 + \frac{d}{d\theta}\beta(\theta)\right]^{-1} \tag{4}$$

and ω_o is the angular frequency of the driving signals.

An approximate analytic expression for the acoustic field B in the focal plane can be derived for the simplified case without modulation ($\beta = 0$) when N is sufficiently large ($N \geq 4m$), and where the array center has been removed to the radius r_o. Assuming the geometry of Fig. 2, the acoustic field is

$$\begin{aligned} B &= \int_{r_o}^{r_1}\int_{o}^{2\pi} A(\theta)\exp j\left[k_f r\cos(\theta-\Psi)\right] r\,d\theta\,dr \\ &= A_o \exp j\left[m\left(\Psi+\frac{\pi}{2}\right)-\omega t\right] \\ &\quad \cdot \int_{r_o}^{r_1}\int_{o}^{2\pi} \exp j(m\theta - k_f r\sin\theta) r\,d\theta\,dr \\ &= 2\pi A_o \exp j\left[m\left(\Psi+\frac{\pi}{2}\right)-\omega t\right]\int_{r_o}^{r_1} J_m(k_f r) r\,dr \end{aligned} \tag{5}$$

where $k_f = kR/Z_f$. Equation (5) can be approximated by

$$B = A_o \exp j\left[m\left(\Psi+\frac{\pi}{2}\right)-\omega t\right]\pi\left(r_1^2 - r_o^2\right) J_m(k_f r_2) \tag{6}$$

where

$$r_2 = \frac{2}{3}\frac{r_1^3 - r_o^3}{r_1^2 - r_o^2}.$$

Equation (6) shows that the field has a shape determined by the mth order Bessel function. Thus, the vortex-shaped field is zero along the central axis for $m \neq 0$ and has a diameter proportional to the vortex mode m (and phase velocity ω_p).

When β is nonzero, a form of spatial frequency modulation exists around the transducer disk. Numerical computations of the fields produced in the focal plane with this form of phasing shows that, for certain phase modulation functions β, the focal annuli are enlongated along one axis producing heating patterns that are ellipsoidal shaped. Factors determining optimum choice of both m and $\beta(\theta)$ are currently being studied. Some typical field patterns will be shown herein.

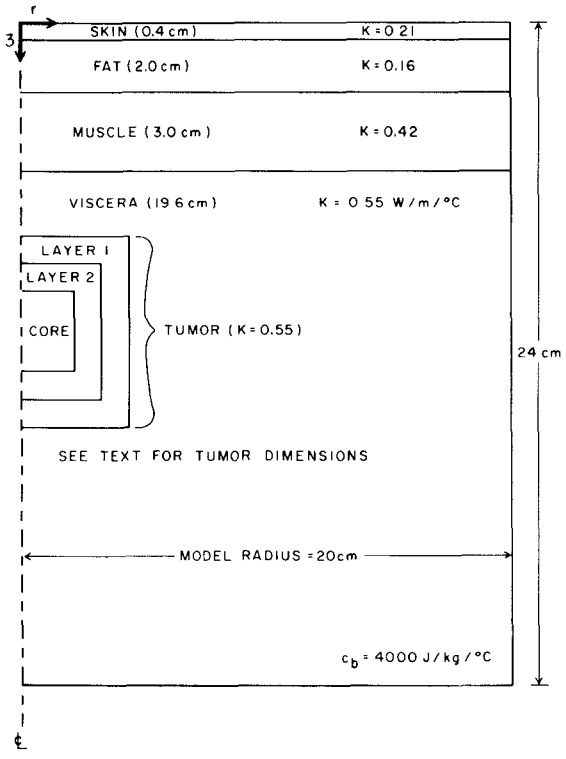

Fig. 3. Geometry of cylindrical model used for thermal calculations. A half-cylinder cross section is shown.

III. Methods

A. Computation of Ultrasonic Field Patterns

The transducer surface is numerically subdivided into discrete elements with element centers separated by less than $\lambda/4$. All transducers studied herein have circular symmetry, thus the separation procedure is to divide the applicator first into concentric rings with each ring segmented by appropriate circumferential divisions. Each discrete element is assigned a complex drive amplitude according to the phasing conditions of the particular applicator under study. The acoustic field is then computed at appropriate grid points in the plane of interest by summing the complex amplitudes for all discrete transducer elements as modified by attenuative propagation from element point to grid point. Attenuation is assumed to be 1 dB/cm/MHz. This simple numerical approach, while inefficient on conventional computers, results in computed field patterns in reasonable times when implemented on a machine capable of rapid parallel processing (HITAC S-810, Hitachi, LTD.).

B. Thermal Modeling

To simulate the thermal response of tumors to the annular-shaped focal regions produced by the applicators discussed herein, a finite difference technique was used to solve the bioheat equation in two-dimensional (r, z) cylindrical coordinates using the geometry illustrated in Fig. 3. In the steady state neglecting metabolic heat generation, the appropriate bioheat equation [16] in cylindrical coordi-

nates is

$$\frac{\partial^2 T}{\partial r^2}+\frac{1}{r}\frac{\partial T}{\partial r}+\frac{\partial^2 T}{\partial z^2}+\frac{q}{K}+\frac{W_b c_b}{K}(T_b-T)=0 \quad (7)$$

where K is the thermal conductivity (W/m/°C), T is the tissue temperature (°C) at coordinates (r, z), W_b is the blood perfusion rate (Kg/m^3/s), c_b is the blood specific heat (J/Kg/°C), T_b is the arterial blood temperature, and q is the power deposition [W/m^3] at coordinates (r, z). The output of the ultrasonic field pattern program $q(r, z)$ is the input to the finite difference form of (7), which is then solved using the method of successive displacements with over-relaxation [17].

The thermal properties and dimensions of the normal and tumor tissues used in the computations are modified from Roemer *et al.* [16]. A surface temperature of 25°C and a temperature along the bottom surface and outer sides of the cylindrical model of 37°C served as boundary conditions for all computations. W_b, for all normal tissue, was assumed to be 8.3 Kg/m^3/s. Tumor blood flows and tumor dimensions are specified where the numerical solutions of (7) are given.

IV. Results

In what follows, an operating frequency of 0.5 MHz is assumed. Tissue attenuation in all computations was 1 dB/cm/MHz. Aperture rings were assumed to be separated (center to center) by less than $\lambda/4$.

A. Concentric-Ring Array

Field patterns were computed for a concentric-ring applicator with an aperture diameter of 12 cm, a focal ring diameter of 6 cm, and a focal length of 8 cm. Fig. 4 illustrates the field intensities in six different planes (transverse planes) parallel to the aperture plane. In the focal plane ($z = 8$ cm), a well-behaved focal annulus is generated which would produce minimal power absorption outside the heating annulus. In a plane intermediate between the aperture and the focal plane ($z = 4$ cm), the peak intensity of the annulus decreases and the annular width is broadened giving a somewhat cone-shaped heating pattern. In planes distal to the focal plane, the peak intensity of the annulus decreases rapidly and the secondary on-axis "focus" increases until it eventually exceeds the peak intensity of the focal plane annulus. This behavior is illustrated more quantitatively in Fig. 5 which gives in the primary longitudinal plane both a contour plot (Fig. 5(a)) and a three-dimensional "bird's eye" view (Fig. 5(e)) of the field intensities. Fig. 5(b) shows the "longitudinal maximum projection" (maximum intensity to be found along the appropriate transverse line.) This shows clearly how the secondary focus intensity exceeds the peak intensity of the focal plane annulus. Fig. 5(c) shows the projection of the focal plane intensity while Fig. 5(d) shows the "transverse maximum projection." These projections (Figs. 5(b), (c), and (d)) are normalized to the absolute peak intensity

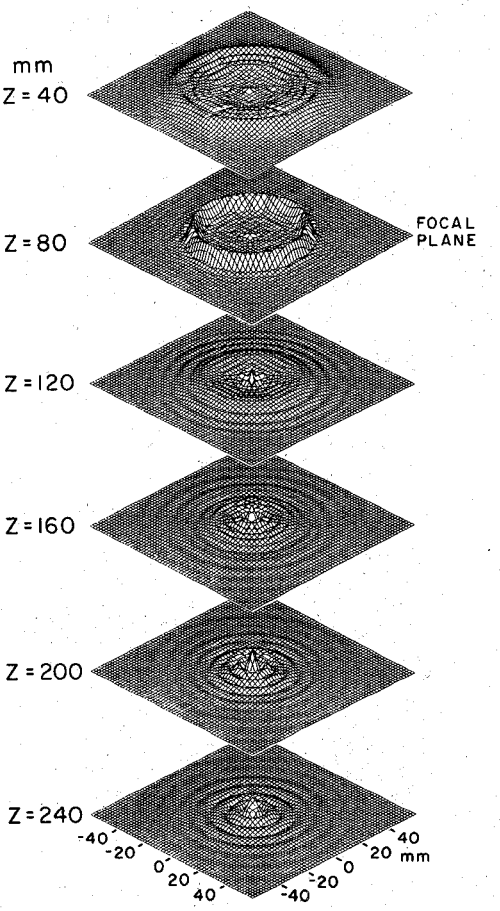

Fig. 4. Concentric-ring applicator intensity patterns in six transverse planes. All intensities shown are normalized to the maximum intensity produced by this configuration. Applicator diameter is 12 cm, focal diameter is 6 cm, and the focal plane is 8 cm from the aperture plane.

which is located in the secondary focal region about 18 cm from the aperture surface.

It is obvious from Figs. 4 and 5 that the secondary focus may produce a "hot-spot" sufficiently intense to be of concern in some hyperthermia applications, particularly if bone is distal to the tumor. However, this region is quite narrow and may produce acceptably low peak temperatures in regions of normal blood perfusion (discussed later). The secondary focus also can be significantly reduced by several phasing techniques. As first discussed by Beard *et al.* [9], if the outer edge of a fixed lens annular focus transducer is masked by absorbing rubber, the intensity of the secondary focus is significantly reduced. This is illustrated in Fig. 6 which shows field intensities with the same phasing as in Figs. 4 and 5 except that the outer transducer rings (beyond a radius of 4.5 cm) are unexcited. This is equivalent to an absorbing masking ring with a 1.5 cm width. Note (Fig. 6) that the intensity of the secondary focus along the entire primary axis is reduced and spread out in space as compared to the nontruncated applicator (Figs. 4 and 5). Moreover, outer edge truncation also changes the shape of the "heating cone" proximal to the focal plane producing a more cylindrical and less-cone-

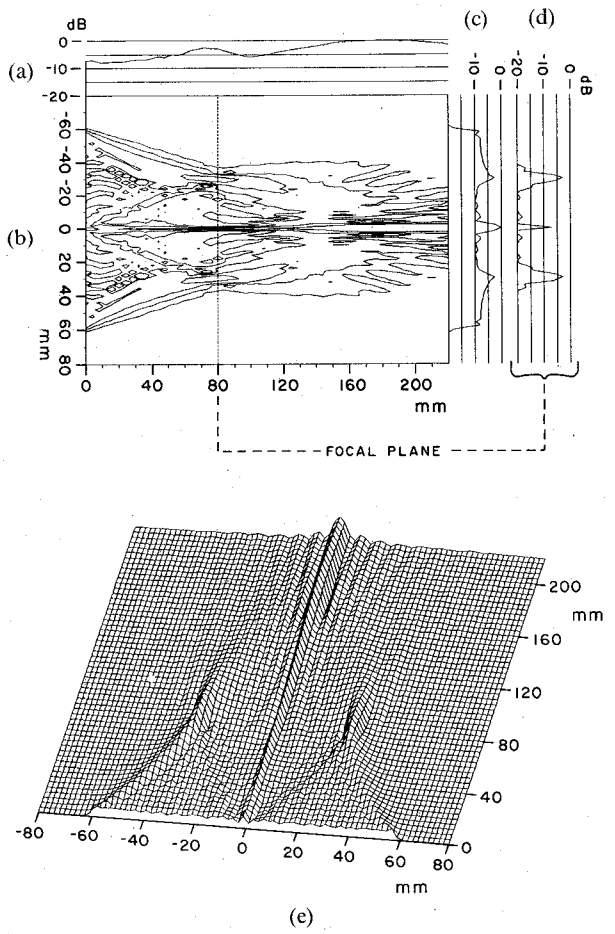

Fig. 5. Concentric-ring applicator intensity patterns. (a) Contour plot with contour increments of 5 dB. (b) Longitudinal projection of the maximum intensity. (c) Projection of intensity in the focal plane. (d) Transverse projection of maximum intensity. (e) "Bird's eye" view.

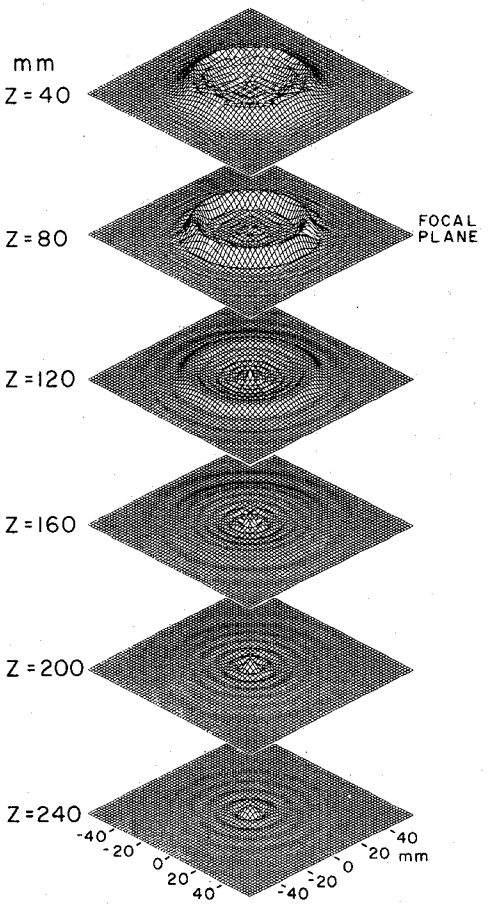

Fig. 6. Truncated or "masked" concentric-ring applicator (see text) intensity patterns in six transverse planes. Applicator diameter is 9 cm, focal diameter is 6 cm, and the focal plane is 8 cm for the aperture plane.

shaped heating region. The enlongated focal region may allow some tumors to be heated with a minimum of scanning of the focal plane depth. On the other hand, this heating shape may present surface heating problems in some applications.

Fig. 7 shows in more quantitative form the field patterns for the truncated or "masked" applicator. In particular, Figs. 7(b), (c), (d), and (e) illustrate the reduction in the intensity of the secondary focal region. Comparison of the "bird's eye" views of Fig. 5(e) and Fig. 7(e) shows clearly the spreading out of the secondary focus caused by truncation and the change in shape of the heating region near the applicator surface.

Another technique has been developed to reduce and spread out in space the energy directed along the primary axis. This can be accomplished by the sector-vortex applicator (Fig. 2) in combination with the concentric-ring applicator. This combination will be considered after the following section on sector-vortex applicators.

The concentric-ring array offers considerable flexibility in providing heating annuli which can be scanned in diameter and in focal length. Thus, when a larger tumor is heated, the periphery as well as the interior can be treated with a scanning pattern tailored to maintain a therapeutic temperature throughout the tumor volume. A limit, however, is reached for small diameter regions. If an annulus of small diameter is attempted by the concentric-ring method, one rapidly approaches a pattern that is simply a single-focus transducer, i.e., the "secondary" focus predominates. This can be seen by observing the form of (1) as R approaches zero $\cdots$ it approaches the phase distribution ϕ_k necessary to generate a single focal region. However, the generation of small diameter focal regions can be accomplished by the sector-vortex array, the topic of the next section.

B. Sector-Vortex Array

An array was studied with the structure given in Fig. 2 with the phasing given by (2). If $\beta(\theta)$ of (2) is set to zero, then intensity patterns from the array will have circular symmetry. Fig. 8 shows the intensity patterns in four planes ($z = 4$, 8, 12, and 16 cm) for four different vortex modes ($m = 0, 4, 8, 12$). The aperture diameter is assumed to be 12 cm. The central disk of diameter 4 cm is unexcited resulting in a central hole (doughnut-shaped applicator). The fixed (or concentric ring-phased array) lens has a focal length of 8 cm with focal radius equal to zero (single

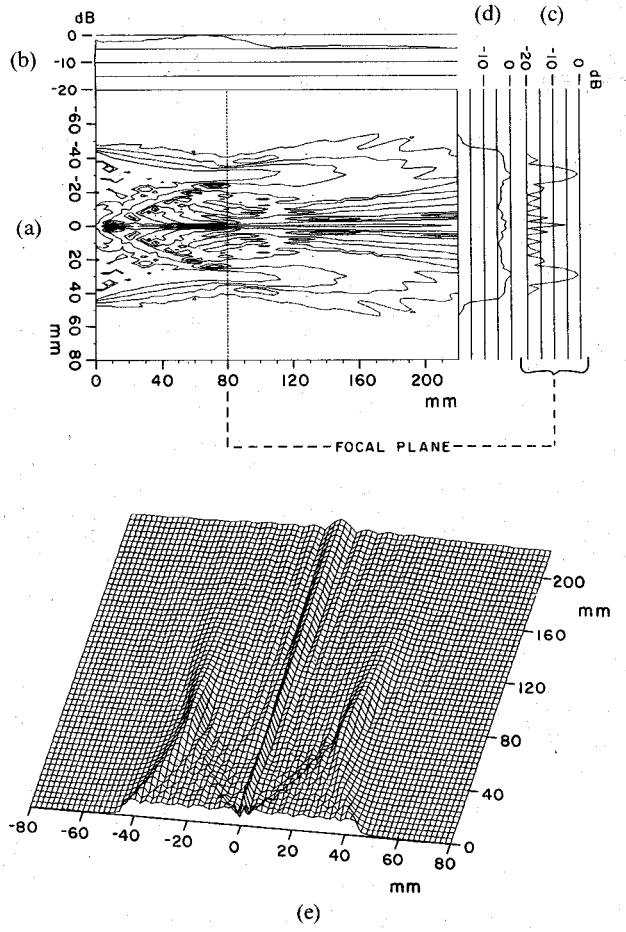

Fig. 7. Truncated concentric-ring applicator intensity patterns. (a) Contour plot (5-dB increments). (b) Longitudinal maximum intensity projection. (c) Projection of focal plane intensity. (d) Transverse maximum intensity projection. (e) "Bird's eye" view.

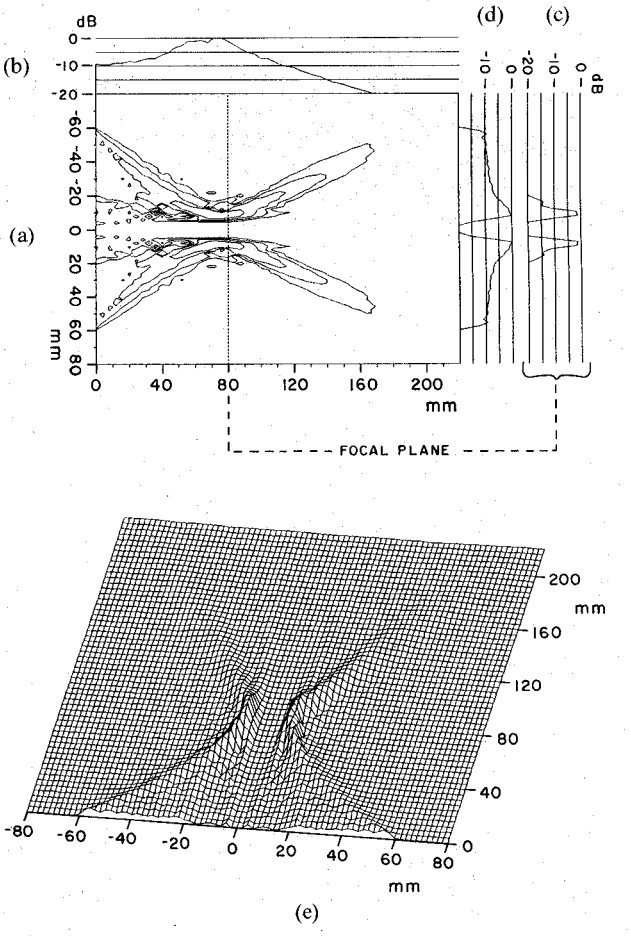

Fig. 9. Sector-vortex intensity pattern for $m = 8$. (a) Contour plot (5-dB increments). (b) Longitudinal maximum intensity projection. (c) Projection of focal plane intensity. (d) Transverse maximum intensity projection. (e) "Bird's eye" view. Applicator diameter is 12 cm and the focal plane is 8 cm from the aperture plane.

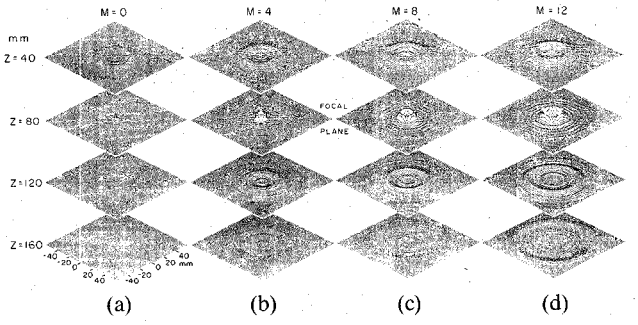

Fig. 8. Sector-vortex applicator intensity patterns in four transverse planes. (a) $m = 0$. (b) $m = 4$. (c) $m = 8$. (d) $m = 12$. Applicator diameter is 12 cm and the focal plane is 8 cm from the aperture plane.

focus). By creating the rotating excitation field ($m \neq 0$), small diameter annuli are created as shown in Fig. 8. When $m = 0$, this is equivalent to a single focus transducer with the pattern in Fig. 8(a). As the vortex mode increases, the diameter of the generated annuli also increases as predicted by the approximate analytical expression given by (6). An interesting and useful feature of the patterns for nonzero vortex mode is that the central axis intensity is everywhere zero. The resulting pattern resembles a "double-funnel" with the peak intensity occurring at the point of maximum constriction or minimum diameter.

Fig. 9(a) gives the contour plot for the applicator of Fig. 8(c) ($m = 8$). Note the well-behaved intensity pattern in the focal plane (Fig. 9(c)). Fig. 9(b) also shows that the maximum projection along the axial direction is also well-behaved with the peak intensity occurring very near the focal plane. The "double-funnel" vortex-shaped field is illustrated in Fig. 9(e).

If $\beta(\theta)$ of (2) is nonzero, then we have asserted that an elongated annular heating field pattern can be generated. Fig. 10(a) shows the intensity in the focal plane ($z = 8$ cm) with a sector-vortex applicator physically identical to that which produced the patterns of Figs. 8 and 9. Only the phasing has been changed, such that the phase distribution is

$$\phi(\theta) = 8\left(\theta + \frac{0.3}{2}\sin 2\theta\right).$$

Here the vortex mode m is 8 and the phase modulation function $\beta(\theta)$ is nonzero. Fig. 10(b) shows the contour plot in the focal plane along with appropriate maximum inten-

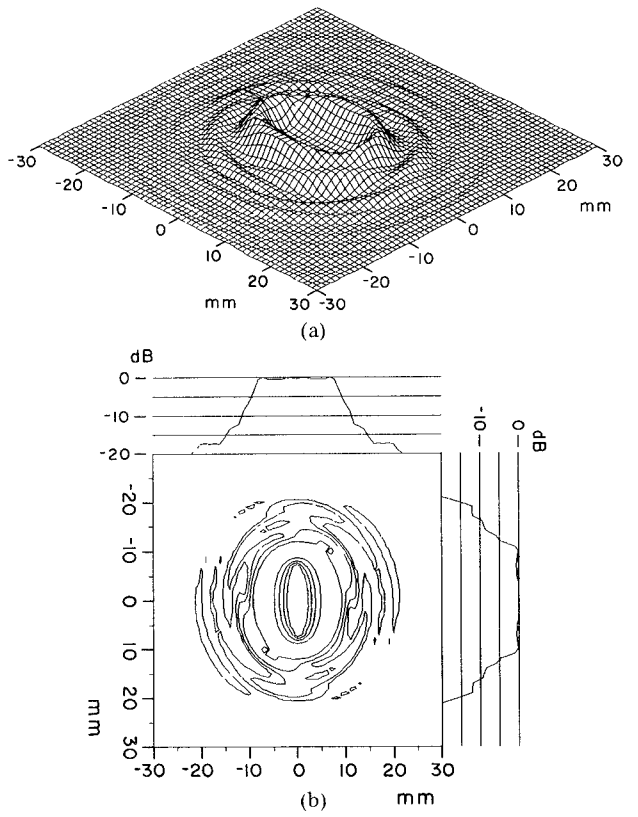

Fig. 10. Sector-vortex intensity patterns for $m = 8$ with phase modulation (see text). (a) Intensity pattern in the focal plane. (b) Contour plot (5-dB increments) in the focal plane. Aperture diameter is 12 cm, focal length is 8 cm, and $\phi(\theta) = 8(\theta + (0.3/2)\sin 2\theta)$.

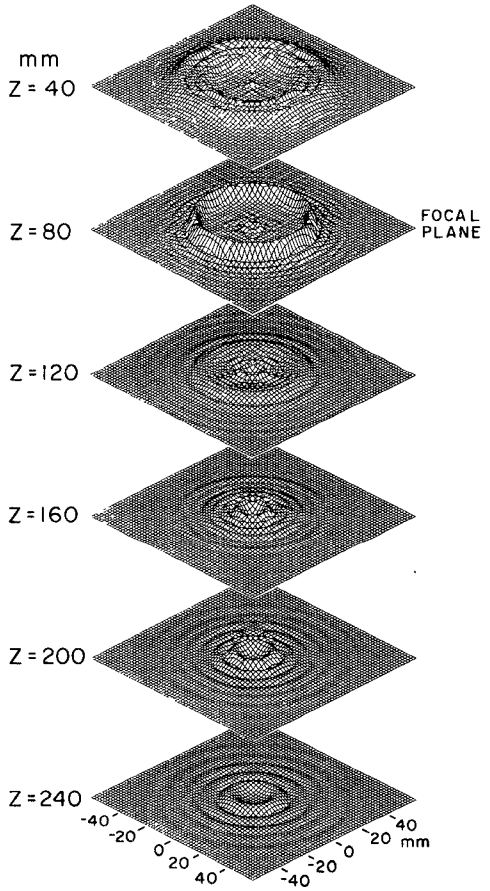

Fig. 11. Combined concentric-ring and sector-vortex applicator intensity patterns in six transverse planes. Applicator diameter is 12 cm, focal diameter is 6 cm, and the focal plane is 8 cm from the aperture. Vortex mode is four ($m = 4$).

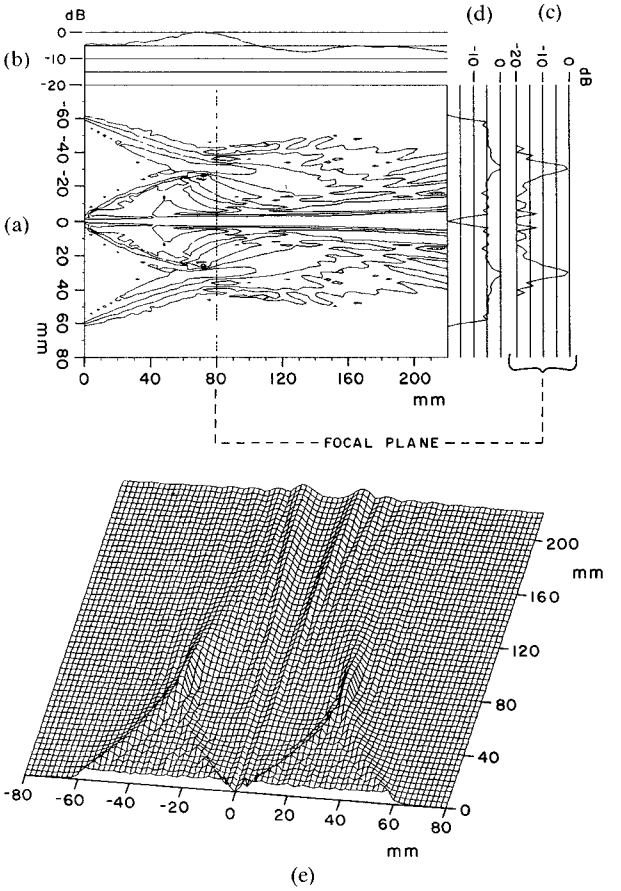

Fig. 12. Combined applicator intensity patterns. (a) Contour plot (5-dB increments). (b) Longitudinal projection of maximum intensity. (c) Projection of focal plane intensity. (d) Transverse maximum intensity projection. (e) "Bird's eye" view.

sity projection curves. Such a pattern might be useful for treating nonspherical tumors.

Thus, with a combination of sector-vortex and concentric-ring arrays, a wide range of heating annuli diameters can be generated. One application of the combined array is illustrated in the next section.

C. Combined Array

A combined array having an aperture diameter of 12 cm with vortex mode $m = 4$ and phase modulation $\beta(\theta) = 0$ gives an intensity pattern illustrated in six serial planes in Fig. 11. The intensity along the primary axis is reduced to zero. The energy, highly concentrated along the axis for concentric-ring arrays, is effectively spread out over a larger volume in the combined mode of operation. Fig. 12(a) shows the contour plot of this applicator. Comparison of Fig. 12(b) to Fig. 5(b) shows that the peak intensity in a direction perpendicular to the array surface occurs near the focal plane in the combined array, but is in the secondary focal region for the concentric-ring array. This is a considerable improvement that only slightly affects the intensity in the focal plane (compare Fig. 5(c) to Fig. 12(c)). The spreading out of the energy in the secondary focus is illustrated in the "bird's eye" view of Fig. 12(e).

D. Thermal Modeling

Physical dimensions of the tumor model are shown in Fig. 13. Blood flow in tumor layer 1 and all normal tissue

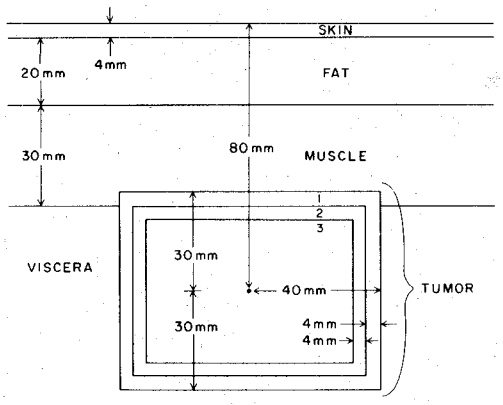

Fig. 13. Physical dimensions of the tumor model used in numerical computations.

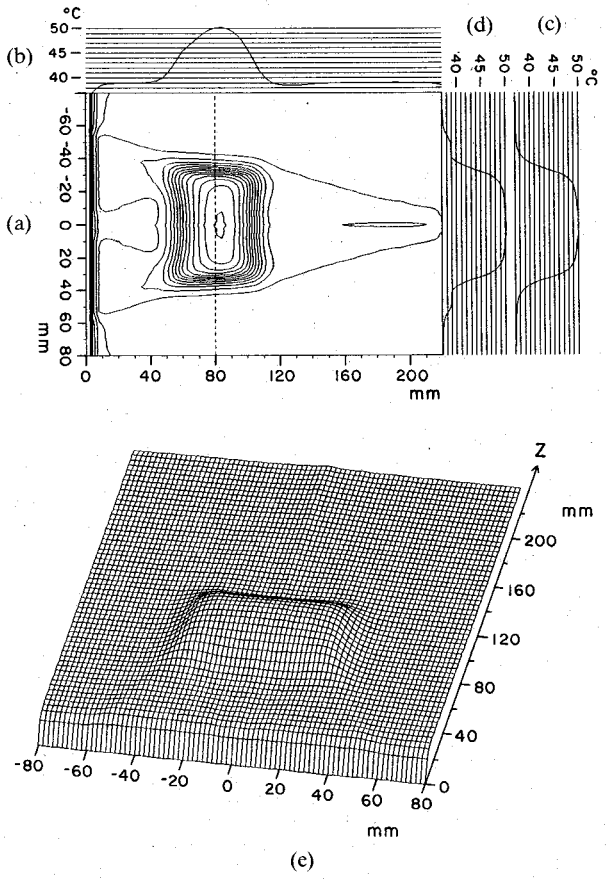

Fig. 14. Temperature distributions for zero tumor blood perfusion assuming a concentric-ring applicator with intensity pattern shown in Figs. 4 and 5. (a) Contour plot (1.0°C contour increments). (b) Longitudinal maximum temperature projection. (c) Projection of focal plane temperature. (d) Transverse maximum temperature projection. (e) "Bird's eye" view of temperature.

was defined to be 8.3 Kg/m^3/s with the middle tumor layer being 2/3 this value (layer 2). Blood flow in the tumor core was assumed to be 1/3 that of normal tissue. In some computations, the blood perfusion values in all three regions are scaled by a constant factor varying from zero to unity. The peak rate of power absorption was 6.4×10^5 W/m^3. Temperatures were computed for the concentric-ring array which produced the intensity pattern illustrated in Figs. 4 and 5.

With zero blood flow in the tumor (scaling factor = 0) the annular intensity pattern of Figs. 4 and 5 results in a computed temperature distribution shown in Fig. 14. Thus,

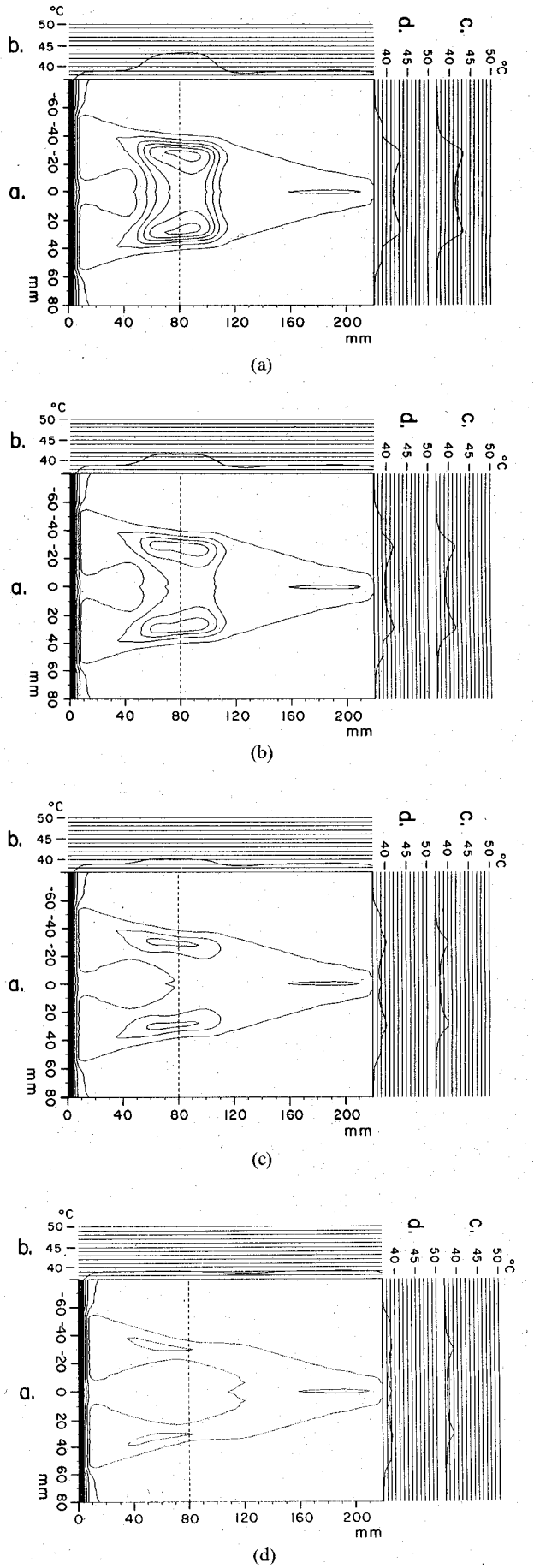

Fig. 15. Tumor temperature contour plots as a function of tumor blood perfusion. (a) Tumor blood perfusion scaling factor = 0.125. (b) 0.250. (c) 0.50. (d) 1.0. (See text for explanation, see Fig. 14 for explanation of panels a–d.)

for poorly perfused tumors, a single annular pattern is sufficient to heat relatively uniformly a significant volume. Note also from Fig. 14(b) that the temperature along the axial direction is not as uniform as in the transverse direction. This may indicate that scanning of the focal length may sometimes be necessary. Also, it should be noted that the temperature in the secondary focal region beyond the focal plane is negligible due to the blood flow of normal tissue in that region and the narrow width of the secondary focus.

Fig. 15 illustrates the effect of increasing tumor blood flow (variation in tumor blood perfusion scaling factor from 0.125 to 1.0). Comparison of Fig. 15(a) and Fig. 14 illustrates clearly the difference that even moderate blood flow can make in temperature distributions. As the blood perfusion scaling factor increases to unity (Figs. 15(b), (c), and (d)), the maximum tumor temperature (for the same power input) decreases dramatically along with the shape of the temperature distribution. Clearly, for highly perfused tumors, a single annular heating region is insufficient to produce acceptable therapeutic temperature distributions. Scanning of the heating annulus diameter, however, would allow the cooled central region to be heated. Significantly more power input also would be required.

V. Discussion

The concentric ring array can produce useful annular heating patterns with diameters ranging from approximately $0.25D$ to about $0.8D$ where D is the applicator diameter. Moreover these annuli can be scanned in diameter and focal length for additional heating flexibility. Unfortunately, this type of applicator generates a strong secondary focus along the central axis. This secondary focus, first described by Beard *et al.* [9] for the fixed lens case, can become quite intense (see Fig. 5). Several methods are possible for reducing this central hot spot. Beard *et al.* pointed out that "masking" the annular focus transducer along the outer rim with absorbing rubber reduces the secondary focus considerably. This "masking," which results in balancing of field contributions from the center with those from the edge of the applicator, is easily accomplished with appropriate phasing producing the results shown in Fig. 6. Another method to reduce the central hot spot is to combine the concentric-ring and sector-vortex arrays. This theoretically reduces the intensity along the control axis to zero. In effect, the energy of the secondary focus is spread out over a much larger volume (see Fig. 11), reducing the probability of producing unwanted hot spots which might damage normal tissue.

The sector-vortex array, in conjunction with geometric focusing, produces useful annular patterns at depth with diameters ranging from zero (single focus transducer) to approximately $0.4D$, thus overlapping and extending to smaller diameters the range of the concentric-ring array. The sector-vortex array with a fixed (geometric) focus lens is a particularly uncomplicated structure. Although it has a fixed focal length, the depth of focus of the focal region is large (see Fig. 8) and only several such applicators with different fixed focal length lenses might be capable of heating both superficial and deep-seated tumors. If the fixed lens is replaced by a concentric-ring array for changing the focal length by phasing, the versatile two-dimensional sector-ring array results at the cost of more elements and associated driving electronics.

Two approaches to ultrasound-phased array applicator design are currently being studied. Both the "direct synthesis" and the "scanning spot" approaches are capable of generating a wide range of useful heating patterns which can be rapidly changed in response to a rapidly changing thermal environment. In the scanning spot approach, the tissue is effectively heated by a high peak-intensity low duty-cycle acoustic waveform while the direct synthesis approach heats with a continuous wave signal that may vary only slowly in intensity over time. Thus, if nonthermal biological effects of the ultrasound exposure are to be considered (cavitation, etc.), these two approaches may produce identical temperature elevations with quite different thresholds for observation of the biological effects of nonthermal phenomena. In addition, safety considerations between the two methods may be of importance. In the case of the scanning spot approach, a fail-safe mechanism to prevent possible exposure to a static highly intense focal spot would be necessary. In the direct synthesis approach, this potentially dangerous situation is much less likely to occur.

Several areas can be identified where further work on these types of phased arrays may prove fruitful. The generation of heating patterns of noncircular symmetry is possible by modulating the phase velocity of the excitation field that rotates around the sector-vortex array (see Fig. 10). However, more work needs to be done to establish quantitative methods for obtaining appropriate phase modulation functions $\beta(\theta)$ of (2) for different heating situations. More work also needs to be done to determine the minimum number of elements that will give adequate heating performance for different treatment situations. A prototype system currently being implemented may help answer some of these questions. The possibility of using phase and amplitude conjugation techniques for focusing in dissipative media, as suggested for use in microwave-phased array applicators [5], [18], should also be explored. And finally, although all of these array concepts have been discussed in the context of ultrasound hyperthermia applicators, some of the ideas might be usefully applied to the design of microwave arrays, particularly if suitable radiating elements can be designed to emulate the rings and sectors described herein.

VI. Conclusion

The concentric-ring-and sector-vortex-phased arrays are two new approaches to applicator design capable of generating directly annular-shaped heating patterns of the type, which on occasion, have been found to be useful in hyperthermia cancer therapy. In both types of arrays, the diameter of the annular pattern can be rapidly scanned by changing the drive signal phase distribution of the array elements. This flexibility will allow real-time response to rapidly changing tumor thermal parameters during treat-

ment. The sector-vortex array will be useful for treating smaller volumes where the concentric-ring array is ineffective. Larger diameter annular heating patterns can be generated by the concentric-ring array. A combination ring-sector applicator would be capable of generating useful heating patterns over a wide range of treatment situations.

ACKNOWLEDGMENT

This work was performed while Charles Cain was on sabbatical leave at Hitachi Central Research Laboratory in Tokyo, Japan. The support and helpful discussions of K. Katakura are gratefully acknowledged.

REFERENCES

[1] K. B. Ocheltree, P. J. Benkeser, L. A. Frizzell, and C. A. Cain, "An ultrasonic-phased array applicator for hyperthermia," *IEEE Trans. Son. Ultrason.*, vol. SU-31, pp. 526–531, 1984.

[2] K. B. Ocheltree, P. J. Benkeser, L. A. Frizzell, and C. A. Cain, "A stacked linear-phased array applicator for ultrasonic hyperthermia," in *Proc. 1984 IEEE Ultrasonics Symp.*, pp. 689–692, 1984.

[3] P. J. Benkeser, K. B. Ocheltree, L. A. Frizzell, and C. A. Cain, "Ultrasound-phased array hyperthermia applicator," in *Proc. IEEE EMBS Symp.*, Chicago, IL, Sept. 1985.

[4] W. Gee, S.-W. Lee, N. K. Bong, C. A. Cain, R. Mittra, and R. L. Magin, "Focused array hyperthermia applicator: Theory and experiment," *IEEE Trans. Biomed. Eng.*, vol. BME-31, pp. 38–46, 1984.

[5] T. C. Guo, W. W. Guo, and W. E. Larsen, "A local field study of a water immersed microwave antenna array for medical imagery and therapy," *IEEE Trans. Microwave Theory Tech.*, vol. MTT-32, pp. 844–854, 1984.

[6] P. F. Turner, "Hyperthermia and imhomogeneous tissue effects using an annular-phased array," *IEEE Trans. Microwave Theory Tech.*, vol. MTT-32, pp. 874–882, 1984.

[7] P. P. Lele and K. J. Parker, "Temperature distributions in tissues during local hyperthermia by stationary or steered beams of unfocused or focused ultrasound," *Br. J. Cancer*, vol. 45, pp. 108–121, 1982.

[8] H. F. Bowman, "Thermodynamics of tissue heating: Modeling and measurements for temperature distributions," in *Physical Aspects of Hyperthermia*, G. H. Nussbaum, Ed. New York: Amer. Inst. Physics, 1982.

[9] R. E. Beard, R. L. Magin, L. A. Frizzell, and C. A. Cain, "An annular focus ultrasonic lens for local hyperthermia treatment of small tumors," *Ultrasound Med. Biol.*, vol. 8, pp. 177–184, 1982.

[10] P. Fessenden, E. R. Lee, T. L. Anderson, J. W. Strohbehn, J. L. Meyer, T. V. Samulski, and J. B. Marmor, "Experience with a nultitransducer ultrasound system for localized hyperthermia of deep tissues," *IEEE Trans. Biomed. Eng.*, vol. BME-31, pp. 126–135, 1984.

[11] P. P. Lele, "Letter: An annular-focus ultrasonic lens for production of uniform hyperthermia in cancer therapy," *Ultrasound Med. Biol.*, vol. 7, pp., 191–193, 1981.

[12] C. B. Burckhardt, P. A. Grandchamp, and H. Hoffman, "Methods for increasing the lateral resolution in B-scan," in *Acoustical Holography*, vol. 5, P. Green, Ed. New York: Plenum, 1974.

[13] J. P. Do-Huu and P. Hartemann, "Annular array transducer for deep acoustic hyperthermia," *Ultrasonics Symp. Proc.*, IEEE-81 CH 1689-9, pp. 705–710, 1981.

[14] J. P. Do-Huu and P. Hartemann, "Deep and local heating induced by an ultrasound-phased array transducer," *Ultrasonics Symp. Proc.*, IEEE-82 CH 1823-4, pp. 735–738, 1982.

[15] P. J. Benkeser, "Investigations of linear phased arrays for hyperthermia applications," M.S. Thesis, Univ. of Illinois at Urbana-Champaign, 1983.

[16] R. B. Roemer, W. Swindell, S. T. Clegg, and R. L. Kress, "Simulation of focused, scanned ultrasonic heating of deep-seated tumors: The effect of blood perfusion, *IEEE Trans. Son. Ultrason.*, vol. SU-31, pp. 457–466, 1984.

[17] G. E. Forsythe and W. R. Wasow, *Finite Difference Methods for Partial Differential Equations.* New York: Wiley, 1960.

[18] H. Ling and S. W. Lee, "Focusing of electromagnetic waves through a dielectric interface," *J. Opt. Soc. Am.*, vol. 1, pp. 965–973, 1984.

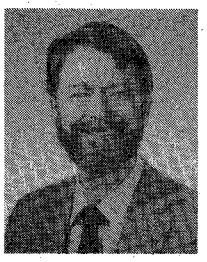

Charles A. Cain (S'65–S'71–M'71–SM'80) was born in Tampa, FL, on March 3, 1943. He received the B.E.E. (highest honors) degree from the University of Florida, Gainesville, in 1965, the M.S.E.E. degree from the Massachusetts Institute of Technology, Cambridge, in 1966, and the Ph.D. degree in electrical engineering from the University of Michigan, Ann Arbor, in 1972.

During 1965–1968, he was a member of the Technical Staff at Bell Laboratories, Naperville, IL, where he worked in the electronic switching systems development area. Since 1972, he has been in the Department of Electrical and Computer Engineering, University of Illinois at Urbana-Champaign, where he is currently Professor of Electrical Engineering and Bioengineering and Chairman of the Bioengineering Faculty. He has been involved in Research on the biological effects and medical applications of microwaves and ultrasound. He is currently an Associate Editor of *Radiation Research*.

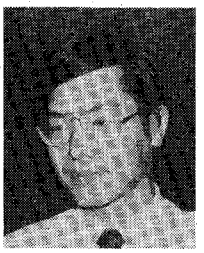

Shin'ichiro Umemura was born in Osaka, Japan, on June 26, 1952. He received the B.E., M.S.E., and Ph.D. degrees in applied physics from the University of Tokyo, in 1975, 1977, and 1980, respectively.

He is currently a member of the Research and Development Staff of the Central Research Laboratory of Hitachi, Ltd., in Kokubunji, Tokyo. He specializes in ultrasound diagnostic array analysis and design and holds a number of patents in this area. He is also interested in the use of ultrasound for the treatment of cancer.

He is a member of the Institute of Electronics and Communication Engineers of Japan, the Japanese Society for Ultrasound in Medicine, and the Japanese Society of Hyperthermic Oncology.